

Operation of the Airborne 355-nm High Spectral Resolution and Doppler Lidar LNG

Didier Bruneau, Jacques Pelon, F. Blouzon, Quitterie Cazenave, Hélène Collomb, Abdanour Irbah, Jean-François Mariscal, Julien Delanoë

▶ **To cite this version:**

Didier Bruneau, Jacques Pelon, F. Blouzon, Quitterie Cazenave, Hélène Collomb, et al.. Operation of the Airborne 355-nm High Spectral Resolution and Doppler Lidar LNG. EPJ Web of Conferences, 2020, The 29th International Laser Radar Conference (ILRC 29), 237, pp.06011. 10.1051/epjconf/202023706011 . insu-02899059

HAL Id: insu-02899059
https://insu.hal.science/insu-02899059

Submitted on 14 Jul 2020

HAL is a multi-disciplinary open access archive for the deposit and dissemination of scientific research documents, whether they are published or not. The documents may come from teaching and research institutions in France or abroad, or from public or private research centers.

L'archive ouverte pluridisciplinaire **HAL**, est destinée au dépôt et à la diffusion de documents scientifiques de niveau recherche, publiés ou non, émanant des établissements d'enseignement et de recherche français ou étrangers, des laboratoires publics ou privés.

OPERATION OF THE AIRBORNE 355-NM HIGH SPECTRAL RESOLUTION AND DOPPLER LIDAR LNG

D. Bruneau (1), J. Pelon (1),

F. Blouzon (2), Q. Cazenave (1), H. Collomb (1), A. Irbah (1), J-F Mariscal (1), J. Delanoë (1)

1 – LATMOS, Sorbonne Université-CNRS-UVSQ Paris, 2DT-INSU, CNRS, Meudon, France

ABSTRACT

High spectral resolution lidar (HSRL) are known to offer capabilities of separating attenuated aerosol and molecular backscattering so that particle extinction and backscattering can be separately retrieved. UV operation provides high energy in eye-safety conditions. Further to that, it could be important for most meteorological or environmental studies to get wind measurements at the same time. LNG is now the only HSR Doppler Lidar (HSRDL) system capable of this. Results obtained during ground-based and airborne measurements show that the backscatter and extinction coefficients at 355 nm can be measured with a relative precision better than 10% (adjusting altitude and time resolution from 60 m to 240 m and 30s to 2mn, respectively) in aerosol layers of 0.5 10^{-6} m^{-1} sr^{-1} backscatter coefficient from ground and aircraft. The same relative precision is obtained in cirrus clouds of a 10^{-5} m^{-1} sr^{-1} backscatter coefficient. The capacity of the system to perform wind velocity measurements has also been demonstrated with precisions in the range of 1 to 2 ms^{-1} in same conditions. We present the main characteristics and illustrate observational capabilities from ground-based and airborne measurements.

I. Instrument

The High Spectral Resolution (HSR) lidar technique allows to differentiate molecular and particular scattering thus improving aerosol or cloud extinction and backscatter coefficients retrieval which are critical parameters for environmental and meteorological studies. The first airborne HSR lidar systems were developed at DLR in Europe [1] and NASA in the USA [2]. The LNG system is based on the use of a Mach–Zehnder interferometer (MZI) as a spectral discriminator [3,4]. This presents the advantage to not require any frequency locking between the emitter and the interferometer and is moreover compatible with a multimode laser emission [5].

Measurement method, system description and first results can be found in [3,6]. We focus here on new results from ground-based and airborne field experiments presenting both scattering and wind measurements.

LNG is a three-wavelength (1064 nm, 532 nm and 355 nm) backscatter lidar with polarization analysis at 355 nm. The HSR capability, based on a MZI, has been added at 355 nm following a previous concept analysis [3]. The lidar is designed to be installed in the Falcon 20 or ATR 42 aircraft of SAFIRE, the French research aircraft service.

A. Emitter

The emitter is based on a Quantel Nd:YAG Q-Switched oscillator, injection seeded with a CW narrow-line emission. It provides single longitudinal mode pulses with 7 ns duration and a 70 MHz linewidth. The fundamental infrared emission is directed though second and third harmonic generators and then through a beam expander. The emitted energy at 355 nm is about 50 mJ@20 Hz, with a divergence smaller than 0.2 mrd. at the beam expander output. The divergence at 532 and 1064 is larger (4 and 5.5 mrd, respectively, to reduce eye-safety distance to a few hundred meters.

B. Receiver

The backscattered light is collected by a Cassegrain telescope with a 300 mm aperture. Behind the telescope focus, an optical package (receiving optics, RO) ensures the separation of the wavelengths, the background light spectral and spatial filtering and the parallel and cross polarization separation at 355 nm. The receiver field-of view is increased at 532 and 1064nm, accordingly to emission. This difference in field-of-views allows particle size estimates from multiple scattering analyses.

C. MZI design

The actual MZI design, detailed in [6], has an optical path difference (OPD) Δ= 20 cm and is field compensated in order to accept the large fiber diameter input without reduction of interference contrast. The MZI optical components and the detectors are mounted in a temperature stabilized box (+/- 0.1°C).

© The Authors, published by EDP Sciences. This is an open access article distributed under the terms of the Creative Commons Attribution License 4.0 (http://creativecommons.org/licenses/by/4.0/).

II. Measurement principle

According to (3), the signal delivered by each channel, for i = 1 to 4, can be written

$$S_i = \frac{S_t}{4} a_i \left[1 + M_i M_a sin\left(\varphi + (i-1)\frac{\pi}{2}\right)\right] \qquad (1)$$

with S_t the total signal, and a_i, M_i the relative photometric sensitivity and instrumental interference contrast of channel i, respectively. M_a is the interference contrast given by the atmospheric backscattered signal and φ the interference phase. The four signals are combined two-by-two in order to produce a complex signal Q (with in-phase and quadrature components), whose modulus is the contrast given by the atmospheric signal:

Always according to [3], the OPD of 20 cm has been chosen so that the interference contrast given by the molecular scattering is null. As the spectral broadening of the particulate scattering is negligible, the resulting contrast is equal to the instrumental contrast produced by the laser itself. Thus, the retrieved contrast M_a is equal to the particulate to total backscatter ratio (PBR) :

$$M_a = |Q| = PBR = \frac{\beta_p}{\beta_m + \beta_p} = \frac{R-1}{R} \qquad (2)$$

where R is the usual lidar backscatter ratio (R=1+βp/βm) and βm, βp are the molecular and particulate backscatter coefficient, respectively. This result is independent of the exact molecular linewidth and line-shape provided it is sufficiently large to yield a null contrast. This avoids the necessity of precise line-shape modeling based otherwise needed [3,4]. Note also that the PBR retrieval is not affected by a Doppler shift of the signal caused by the platform motion and pointing, which is of importance for an airborne instrument.

In addition to the contrast, the interference phase φ, is obtained by the argument of the complex signal Q. Subtracting the reference interference phase φ_r, obtained on a highly attenuated pick-up of the laser emission one can obtain the Line-of-sight particles velocity V_{LOS} with:

$$\varphi - \varphi_r = \frac{2\pi\Delta}{\lambda_0}\left(1 + \frac{2V_{LOS}}{c}\right) \qquad (3)$$

This ensures the Doppler measurement capability with the same MZI device. Of course the phase can only be measured when a significant interference contrast occurs, i.e. on particulate backscattering, but in this case, it is independent of the backscatter ratio.

B. Calibration and signal processing

Before processing actual atmospheric signals, it is necessary to perform a calibration of the MZI for determining the a_i, M_i parameters in Eq. (1). For this purpose we record the reference signal on the 4 channels on long time series. A fit of the recorded signals with the model described by Eq. (1) is obtained with a correlation better than 99.9% that allows determining the a_i and M_i parameters. With an atmospheric density model, we can calculate β_m (only dependent of molecular density) as a function of altitude. The attenuated particulate signal S_{par} and attenuated molecular signal S_{mol} can then be obtained as

$$S_{par} = M_a S_{tot} \quad and \quad S_{mol} = (1 - M_a) S_{tot} \quad (4)$$

with

$$S_{tot} = \frac{4}{M_1^{-1} + M_2^{-1} + M_3^{-1} + M_4^{-1}}\left(\frac{S_1}{a_1 M_1} + \frac{S_2}{a_2 M_2} + \frac{S_3}{a_3 M_3} + \frac{S_4}{a_4 M_4}\right) (5)$$

IV. Scattering measurements

We first present here the measurements performed during tests performed on May 11, 2016 from ground.

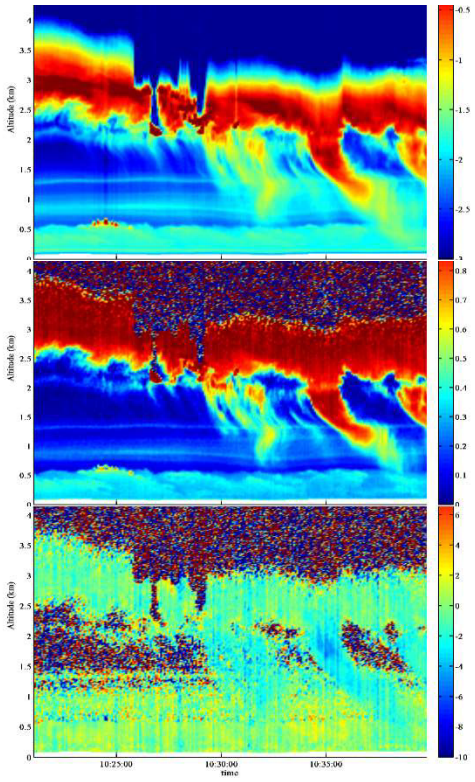


Fig. 1 : (top plot) Time-altitude cross-section of the logarithm of the 1064 nm range-corrected signals showing precipitating altostratus cloud above the 500m high boundary layer ; (middle plot) UV contrast M determined from MZI and (bottom plot) vertical air speed retrieved in the cloud and boundary layer. A 20 mn sequence of G/B measurements is shown for 11 May 2016.

The cross-section of the 1064 nm backscatter signals over the whole test duration is presented in Fig 1 (top panel). The aerosol layers can be clearly identified below 1.5 km from the 1064 nm signal and on the 355 nm MZI contrast. One can see that the boundary layer top is detected from the signal gradient at about 500 m above surface. The contrast M of MZI measurements shows a good dynamics from less than 0.02 to about 1 near cloud top. It allows retrieving the particle backscatter coefficient using Eq. (3). Vertical upward motions are seen in the boundary layer and above, the Doppler shift associated with the precipitations can also be clearly observed.

The 355 nm HSR analysis shows a weak PBR value above the boundary layer, increasing in the cloud up to 0.9, corresponding to an average backscatter ratio = 10 and to a particulate backscatter coefficient of 10^{-1} $km^{-1}.sr^{-1}$. The HSR vertical profiles of particulate backscatter (β_p) and extinction (α_p) coefficients at 355 nm and the related errors (standard deviation) profiles are presented in Fig. 2 for an averaging over 1 minute. The vertical resolutions are 60 m and 240 m for β_p and α_p, respectively. Random errors caused by the detection noise are calculated according to the equations developed in [3], from the total sensitivity of the detection channel and the number of photo-electrons derived from the recorded analog signals.
The particular depolarization ratio varies from 20% to 30% in the cloud. Results show that for long measurement series, the contrast and speed exhibit negligible biases even under variable environmental conditions.

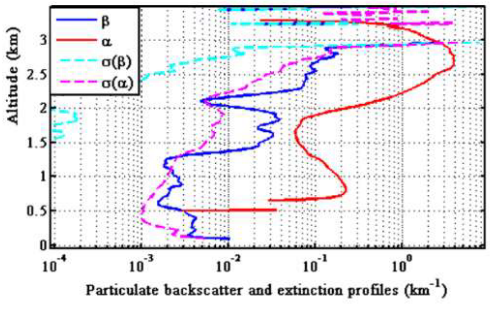


Fig. 2 : Profiles of HSR measurements over the aerosol layer a) particulate backscatter coefficient ($km^{-1}sr^{-1}$) and extinction coefficient (km^{-1}) with related errors (standard deviation).

IV. Airborne measurements

Pointing can be done in nadir or slant viewing (37° inclination angle) modes. We present here the measurements performed in nadir viewing mode during test flights in 2014-2015 and during the NAWDEX/EPATAN field experiment in 2016 [7].

A. Verification of ground echo speed

As a preliminary check of the HSR Doppler performance, measurements of the apparent ground speed Vs during flights over land have shown that the mean difference between the apparent ground speed calculated from the aircraft navigation data and measured by the lidar is 0.1-0.15 ms^{-1} with a standard deviation of about 1.5 ms^{-1}.

B. Cloud microphysics

Flight of 16 October 2016 has been used to perform a multiple field of view analysis. Two ratios are calculated from measured signals: the 532/355nm and the 1064/532 nm. The first one is sensitive to multiple scattering, whereas the second is not due to their similar field of views, and can be used as a reference.

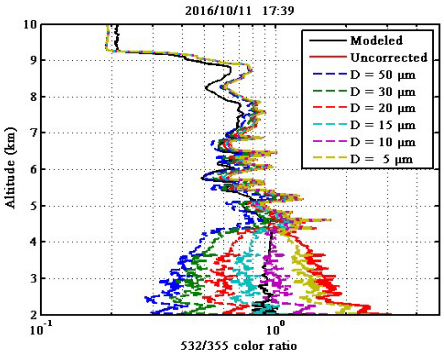


Fig3.: Ratio of the 532 to 355 nm in a mid-level altostratus (below 4.5 km) and calculation using the forward scattering model.

Fig. 3 shows that the correction of the 355/532 nm ratio using the Hogan model [8] allows to bring values close to the 532/1064 nm, indicative of particle size of about 20 µm.

C. Wind speed measurements on VAD

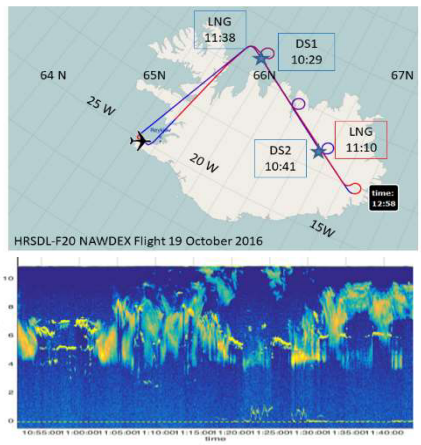


Fig. 3 : Flight plan and circle (top) made by the F20 to perform VAD measurements with LNG in vertical pointing.

Dropsonde launches have been performed on the way to the south-east part of Iceland, whereas VADs have been made on the way back. Backscatter signal in observed cirrus derived from contrast measurements using MZI after roll angle corrections in the four VADs.

During the flight of October 30th, 2016 (track is reported in Fig. 3 (top panel)), the F20 was flying over cirrus clouds over Iceland. Four wind profiles were performed during this flight using the lidar VAD technique on 360° aircraft turns together with two dropsonde launches. Results are presented in Fig. 4.

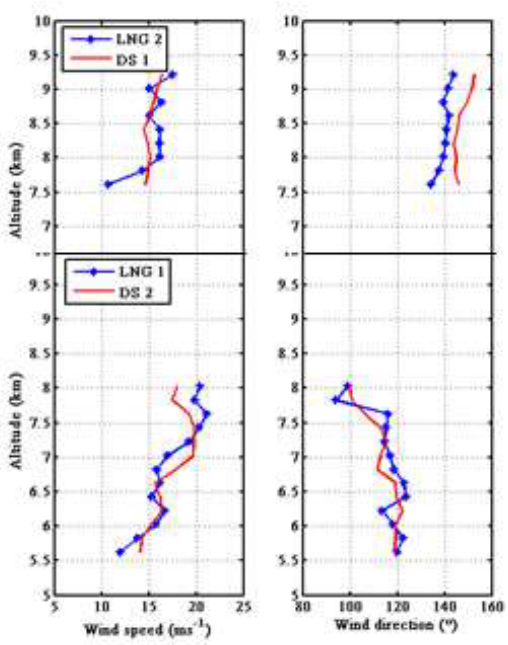


Fig. 4: Vertical profiles of wind speed and direction retrieved from VADs 1 and 3. Note that VAD 3 is closer in time and space to the dropsonde launch.

Comparison between VAD lidar measurement and dropsonde profiles show an excellent agreement, in both wind speed and direction for DS2 closer in time with lidar measurements.

V. Conclusion

The measurement capabilities of the 3-wavelength 2-polarisation HSR Doppler airborne lidar LNG have been successfully demonstrated during field campaigns. Results show that the backscatter and extinction coefficients at 355 nm can be measured with a relative precision of 10% for 60 m and 240 m vertical resolution respectively in aerosol layers of 10-6 $m^{-1}.sr^{-1}$ backscatter coefficient with a 30 km horizontal resolution. The same precision with the same vertical resolution is obtained in cirrus clouds 2 10-5 $m^{-1}.sr^{-1}$ backscatter coefficient with a horizontal resolution of 5 km. The Doppler measurement capability has also been demonstrated. The velocity measurement is performed on the particle backscattering and its precision is strongly dependent on the backscattering ratio. In favorable conditions, LOS wind velocity measurements can be made with a precision in the range of 1 to 2 ms^{-1}. VADs provide accurate profiles of wind components. LOS speed measurements performed on ground echoes show averaged biases less than 0.15 ms^{-1}. This instrument is particularly matched for the cloud studies in combination with cloud radar as planned in the ongoing RALI project [8]. It is planned to be used for aerosol-cloud process studies and for the validation of the ESA space-borne ADM-Aeolus and Earthcare-ATLID lidars. In this frame, further comparisons with ground-based and other airborne instruments are planned to ensure the validation process.

Acknowledgements

Development and test flight of LNG have been supported by INSU and CNES which are acknowledged. The authors also wish to thank the technical support of the Division Technique for the development and flights of the HRSD-LNG and the SAFIRE group for its assistance during the airborne campaign. NAWDEX-EPATAN flights were supported by ESA (Contract No. 4000119015/NL/CT/gp), we particularly acknowledge.

References

[1] M. Esselborn, M. Wirth, A. Fix, M. Tesche, and G. Ehret, "Airborne high spectral resolution lidar for measuring aerosol extinction and backscatter coefficients," Appl. Opt. 47, 346–358 (2008).

[2] J. W. Hair, C. A. Hostetler, A. L. Cook, D. B. Harper, R. A. Ferrare, T. L. Mack, W. Welch, L. R. Izquierdo, and F. E. Hovis, "Airborne high spectral resolution lidar for profiling aerosol optical properties," Appl. Opt. **47**, 6734–6752, (2008).

[3] D.Bruneau and J. Pelon, "Simultaneous measurements of particle backscattering and extinction coefficients and wind velocity by lidar with a Mach–Zehnder interferometer: principle of operation and performance assessment", Appl. Opt., 42, 1101–1114 (2003).

[4] D. Bruneau, A. Garnier, A. Hertzog, and J. Porteneuve, "Wind-velocity lidar measurements by use of a Mach–Zehnder interferometer, comparison with a Fabry–Perot interferometer", Appl. Opt., 43, 1, 173-182, (2004)

[5] D. Bruneau, F. Blouzon, J. Spatazza, F. Montmessin, J.Pelon and B. Faure, "Direct-detection wind lidar operating with a multimode laser", Appl. Opt., 52, 4941-4949, (2013).

[6] D.Bruneau, J. Pelon, F. Blouzon, J. Spatazzan , P. Genau, G. Buchholtz, N. Amarouche, A. Abchiche and O.Aouji, "355 nm high spectral resolution airborne lidar LNG: system description and first results", Appl. Opt. 54, 8776-8785, (2015)

[7] Schäfler and co-authors, The North Atlantic Waveguide and Downstream Impact Experiment, Bull. Amer. Met. Soc., 1607-1637, doi.org/10.1175/, 2018.

[8] Hogan, R. J., 2006: Fast approximate calculation of multiply scattered lidar returns. Appl. Opt., 45, 5984– 5992.

[9] Protat A.; Pelon J., Testud J.; Grand N., Delville P.; Laborie P., Vinson J.-P., Bouniol D.;, Bruneau D.; Chepfer H.; Delanoe J.; Haeffelin M., Noel V. and Tinel C., 2004 : Le projet RALI : Combinaison d'un radar nuage et d'un lidar pour l'étude des nuages faiblement précipitants, La Météorologie, n° 47, 23-33.